Available online at www.sciencedirect.com
SCIENCE DIRECT
Journal of Molecular Catalysis A: Chemical 255 (2006) 109–116
JOURNAL OF MOLECULAR CATALYSIS A: CHEMICAL
www.elsevier.com/locate/molcata

Characterization and photocatalytic activity of Cu-doped $K_2Nb_4O_{11}$

Gaoke Zhang [a,*], Xi Zou [a], Jie Gong [a], Fangsheng He [a], Hao Zhang [a], Shixi Ouyang [b], Hanxing Liu [b], Qiang Zhang [a], Ying Liu [a], Xia Yang [a], Bo Hu [a]

[a] *School of Resources and Environmental Engineering, Wuhan University of Technology, 122 Luoshi Road, Wuhan 430070, PR China*
[b] *State Key Lab of Advanced Technology for Materials Synthesis and Processing, Wuhan University of Technology, 122 Luoshi Road, Wuhan 430070, PR China*

Received 15 February 2006; received in revised form 28 March 2006; accepted 29 March 2006
Available online 11 May 2006

Abstract

The Cu-doped tungsten bronze (TB) type potassium niobate $K_2Nb_4O_{11}$ was synthesized by solid-state reaction method in air. The crystal structure and morphology of the prepared samples were confirmed by X-ray diffraction analysis and scanning electron microscope. The photocatalytic activity of the prepared samples was evaluated using acid red G as a model organic compound and the photocatalytic reaction belongs to the first order kinetics. The results show that Cu-doping significantly increased the photocatalytic activity of $K_2Nb_4O_{11}$ catalyst when the concentration of Cu-doped was lower, but the photocatalytic activity of the catalyst was decreased when the concentration of Cu-doped was higher. Although the surface areas of the 0.2 wt.% Cu-doped $K_2Nb_4O_{11}$ and the 0.5 wt.% Cu-doped $K_2Nb_4O_{11}$ are very lower, the photocatalytic activities of these compounds are close to that of TiO_2–P25. Copper doping is good for the compounds to form tetragonal TB structure and improving the crystallinity of the compounds. The diffuse reflectance spectrum of Cu-doped $K_2Nb_4O_{11}$ showed a red shift. X-ray photoelectron spectroscopy analysis confirmed that the niobium with mixed valence state exists in the crystal structure of the compound $K_2Nb_4O_{11}$. The effects of the Cu-doped and the mixed valence state of niobium on the photocatalytic activity of the catalyst were discussed.

Keywords: Niobate; Cu-doped; Photocatalysis; Degradation; Acid red G; Niobium

1. Introduction

The textile industry produces large quantities of highly colored effluents. Various chemical and physical processes were applied for color removal from textile effluents. One difficulty with these methods, is that they are not destructive but only transfer the contamination from one phase to another, therefore, a new and different kind of pollution is faced which calls for further treatment [1–4]. Recently, semiconductor photocatalysis that costs less money and does not create secondary contamination has become one of the most important technologies for the degradation of organic contaminants in water. Most of the research on semiconductor photocatalysts were focused on TiO_2, which is known as one of the most effective photocatalysts for the degradation of organic pollutants, but its photocatalytic activity is influenced by a wide variety of factors such as, specific surface area, the adsorption affinity and capacity for organic contaminant, electron–hole recombination processes in the bulk and so on [5,6].

In the past two decades, many attentions have been paid for finding more efficient photocatalysts. A variety of niobates had been extensively studied as a new class of photocatalysts in the field of water splitting. Zou et al. [7] reported three photocatalysts Bi_2MNbO_7 ($M = Al^{3+}$, Ga^{3+} and In^{3+}); $InMO_4$ ($M = Nb^{5+}$ and Ta^{5+}) and $BiMO_4$ ($M = Nb^{5+}$ and Ta^{5+}), which could split water into H_2 and/or O_2 under ultra-violet irradiation or visible light ($\lambda > 420$ nm). The photocatalytic activity increases significantly by loading co-catalysts on the surface of the photocatalyst, such as NiO and Pt. Kato and Kudo [8] studied on the photophysical and photocatalytic properties of layered perovskite $Sr_2(Ta_{1-X}Nb_X)_2O_7$. The results showed that the conduction band level of the $Sr_2(Ta_{1-X}Nb_X)_2O_7$ solid solution can be controlled by changing the ratio of niobium to tantalum. The $Sr_2(Ta_{1-X}Nb_X)_2O_7$ solid solution photocatalysts loaded with NiO co-catalysts decomposed water into H_2 and O_2 in a stoichiometric ratio. Domen and Ikeda [9] reported the photocatalytic activities of small particles (0.1–2 μm) of $K_4Nb_6O_{17}$ in water splitting and showed the photocatalytic activity for an overall

* Corresponding author.
E-mail address: gkzhang@mail.whut.edu.cn (G. Zhang).

1381-1169/$ – see front matter © 2006 Elsevier B.V. All rights reserved.
doi:10.1016/j.molcata.2006.03.073

decomposition of water of the Ni-loaded $K_4Nb_6O_{17}$ was twice as high as that for the original catalyst.

These researches described as above were mainly focused on the study of the photocatalytic properties of layered niobates in the field of water splitting. In this paper, we report another new type niobate $K_2Nb_4O_{11}$ used as the photocatalytic degradation dyes, which assumes a tetragonal tungsten bronze (TB) with space group *P4/mbm* (127), and its molecular formula can be written as $K_{5.75}Nb_{10.85}O_{30}$ according to its crystal structure characteristic. The crystal structure of $K_2Nb_4O_{11}$ is constructed by NbO_6 octahedra, which form some triangle, quadrilateral and pentagonal tunnels. The pentagonal and quadrilateral tunnels are occupied by K cations, the triangle tunnels are occupied by Nb cations, and the tunnels make for better import of metal ions [10–12]. Up to now, there are many studies reported on the structures and properties of TB niobates, however, the study of the photocatalytic property of TB niobates in the field of photodegrading the pollution has hardly been reported. It is known that transition metal ions doped into catalysts can increase the quantum efficiency of the heterogeneous photocatalytic property by acting as electron (or hole) traps and by altering the e^-/h^+ pair recombination rate [13]. Copper is a kind of better dopant, Zhang et al. [14] studied copper-doped titanium oxide film. Their results showed copper doping improved the photocatalytic of the film. In this paper, we synthesized the TB potassium niobate $K_2Nb_4O_{11}$ and transition copper ions doped $K_2Nb_4O_{11}$ by solid-state reaction in air. So we would like to discuss the photocatalytic activity of the Cu-doped $K_2Nb_4O_{11}$, and investigate the influence of Cu-doped and the mixed valence state of niobium on the photocatalytic property of these compounds for photodegradation of acid red G.

2. Experimental

2.1. Sample preparation and characterization

The samples of $K_2Nb_4O_{11}$ were prepared by solid state-reaction method. Analytical grade of K_2CO_3, Nb_2O_5 were used as starting materials. The stoichiometric amount of precursors were mixed and pressed into small pellets with an agate mortar. The small pellets were sintered in a crucible at 1000 °C for 2 h, and then cooled to room temperature. The samples for XRD analysis and experiments were prepared by manually grinding the bulk materials to powder with an agate mortar again.

The samples of Cu-doped potassium niobate were also prepared by solid-state reaction; the mixtures of K_2CO_3, Nb_2O_5, and $CuSO_4{\cdot}5H_2O$ were sintered at the same condition.

The structures of the $K_2Nb_4O_{11}$ crystal and Cu-doped $K_2Nb_4O_{11}$ were determined by X-ray diffraction (XRD). X-ray powder diffraction analyses of prepared samples were carried out on a Rigaku D/MAX-RB powder X-ray diffractometer. Scanning electron microscopy (SEM) was performed on JSM-5610LV scanning electron microscope. Surface areas were determined using nitrogen as the sorbate at 77 K in a static volumetric apparatus (Micromeritics ASAP 2010 sorptometer). The samples were previously outgassed at 180 °C for 16 h under a vacuum of 6.6×10^9 bar. The valence state of Nb was analyzed by X-ray photoelectron spectroscopy (XPS), using a VG Scientific ESCALAB Mark II spectrometer equipped with two ultrahigh-vacuum (UHV) chambers; the pressure in the chambers during the experiments was about 10^{-7} Pa. A Mg Kα X-ray source was used. The analyzer was operated at 20 eV pass energy for high-resolution spectra and 50 eV for survey spectra. ESR study was conducted at room temperature with an ESP300E ESR spectrometer (Bruker) in X-band. *g*-Factor values were determined by comparison with an external standard (DPPH, $g = 2.0036$).

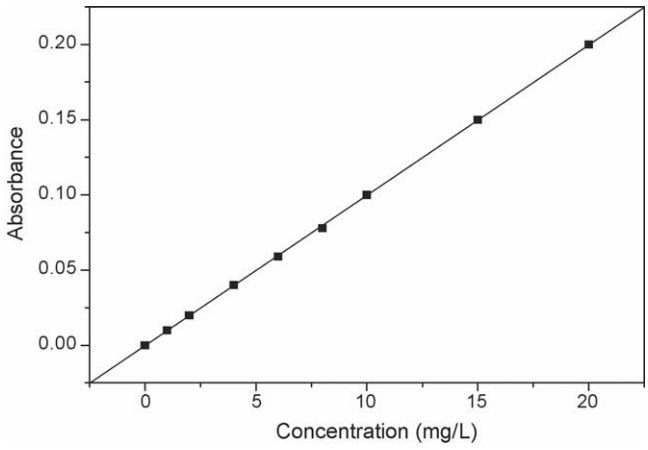

Fig. 1. Standard curve of acid red G at 505 nm (equation: $A = 0.01C - 0.0003 \approx 0.01C$, $R = 0.9999$).

2.2. Photocatalytic experiments

The photodegradation of aqueous acid red G was carried out in a 500 ml beaker with constant magnetic stirring. A commercial 20 W UV lamp was used as the light source. Each as-prepared sample of 150 mg was suspended in 150 ml acid red G aqueous solution (30 mg/L). The distance between the liquid surface and the light source was about 8 cm. The light intensity was about 0.745 mW/cm^2 measured by using an UV-B radiatometer. Sampled the solution six times in 2 h during the photocatalytic process, and the concentration of aqueous acid red G was determined by measuring the absorbance at 505 nm with an UV–vis spectrophotometer and a calibration curve (showed in Fig. 1). The photodegradation rate (X) is given by $X = (C_0 - C)/C_0 \approx (A_0 - A)/A_0$, where C_0 is initial concentration of acid red G, C the concentration at time t and A is the absorbance.

3. Result and discussion

3.1. XRD patterns analysis

X-ray powder diffraction patterns of prepared samples were shown in Fig. 2, the sharp peaks in the XRD patterns indicate a well crystallinity of the prepared samples when calcined at 1000 °C for 2 h. The result of XRD patterns confirmed that the compound $K_2Nb_4O_{11}$ assumes a tetragonal tungsten bronze

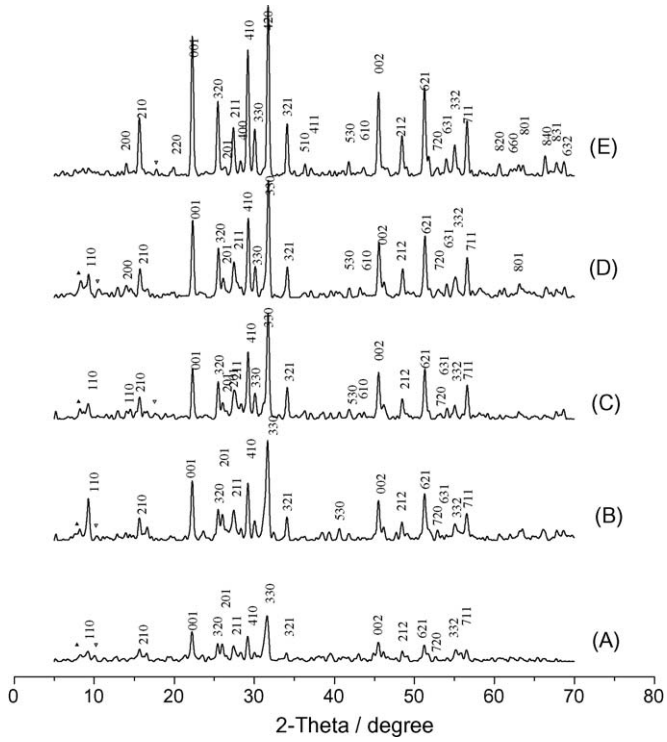

Fig. 2. XRD patterns of the prepared samples: (A) $K_2Nb_4O_{11}$; (B) 0.1 wt.% Cu-doped; (C) 0.2 wt.% Cu-doped; (D) 0.5 wt.% Cu-doped; (E) 1 wt.% Cu-doped; ▲ KNb_3O_8; ▽ $K_3Nb_7O_{19}$.

structure with space group *P*4/*mbm* (127) as that given in JCPDS data card (JCPDS 38-0297) for $K_2Nb_4O_{11}$ crystals. The effect of doped concentration of Cu ions on the crystallization of $K_2Nb_4O_{11}$ were also examined, as shown in Fig. 2, the concentration of Cu-doped has influence on the crystallized of $K_2Nb_4O_{11}$. It is very interesting that all the prepared samples calcined at 1000 °C for 2 h had been well crystallized and the XRD patterns show the crystallinity of the compound increases with increasing the concentration of copper doped in $K_2Nb_4O_{11}$. This indicates that the Cu ions doped $K_2Nb_4O_{11}$ maintains a tetragonal TB structure similar to the $K_2Nb_4O_{11}$ even under extensive modification by Cu ions and copper doping is good for the compounds to form tetragonal TB structure. There is a very small amount of niobate $K_3Nb_7O_{19}$ or KNb_3O_8 in the samples, which have no remarkable influence on the photocatalytic property of these compounds.

3.2. SEM analysis

SEM photographs of $K_2Nb_4O_{11}$ and the 0.2 wt.% Cu-doped $K_2Nb_4O_{11}$ and the 0.5 wt.% Cu-doped $K_2Nb_4O_{11}$ are given in Fig. 3. The morphology of crystals of $K_2Nb_4O_{11}$ is not clear. With increasing the ratio of copper doped in the Cu-doped $K_2Nb_4O_{11}$ compounds, the crystal sizes of the compounds increase and the crystallinity of the compounds becomes well. SEM analysis confirms the result of XRD. The crystal shape of the Cu-doped $K_2Nb_4O_{11}$ compound shows quadrate clearly.

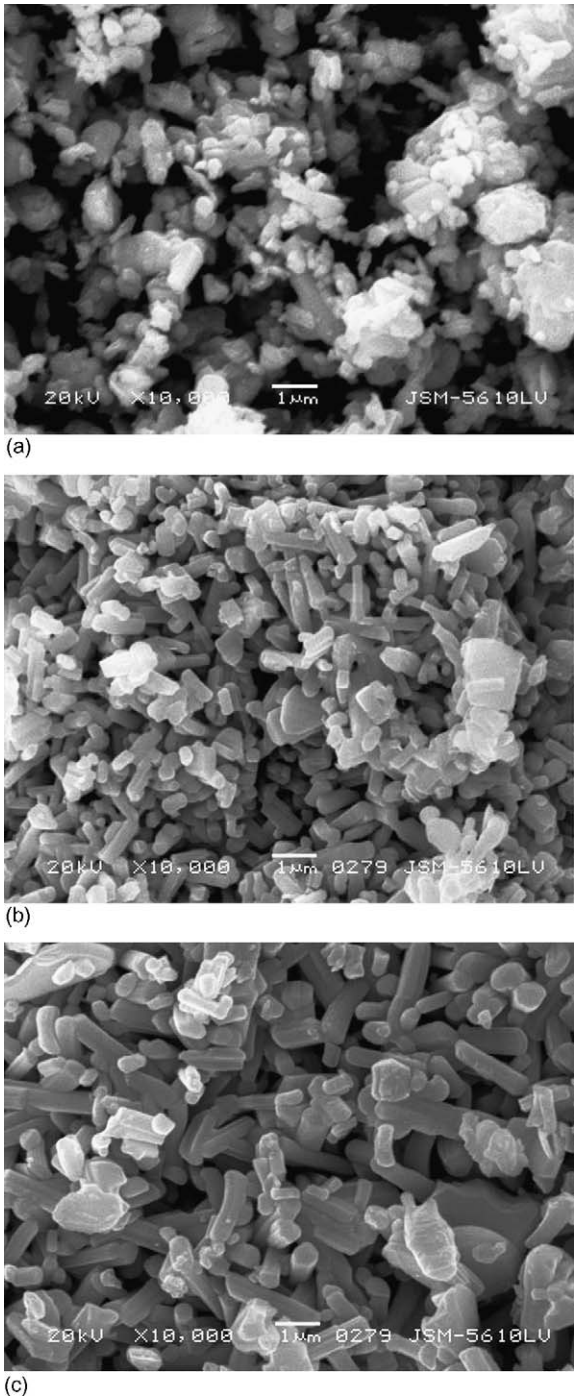

Fig. 3. SEM photographs of the $K_2Nb_4O_{11}$ (a) and the 0.2 wt.% Cu-doped $K_2Nb_4O_{11}$ (b) and the 0.5 wt.% Cu-doped $K_2Nb_4O_{11}$ (c).

3.3. Photocatalytic activity of the catalysts

3.3.1. UV–vis spectra changes

The changes in the absorption spectra of acid red G solution during the photocatalytic process by the Cu-doped $K_2Nb_4O_{11}$ at different irradiation time were recorded by UV–vis spectrometer (UV-160) to determine if any stable chromophoric intermediaters were formed during acid red G degradating (shown in Fig. 4). Before irradiation, the absorption spectra show three

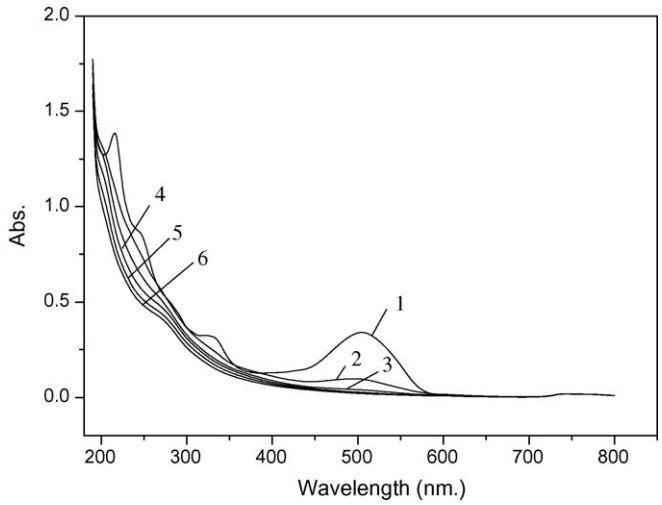

Fig. 4. UV–vis spectra profile changes of photocatalytic degradation of 30 mg/L acid red G by Cu-doped $K_2Nb_4O_{11}$ at different times: (1) zero; (2) 20 min; (3) 40 min; (4) 60 min; (5) 90 min; (6) 120 min.

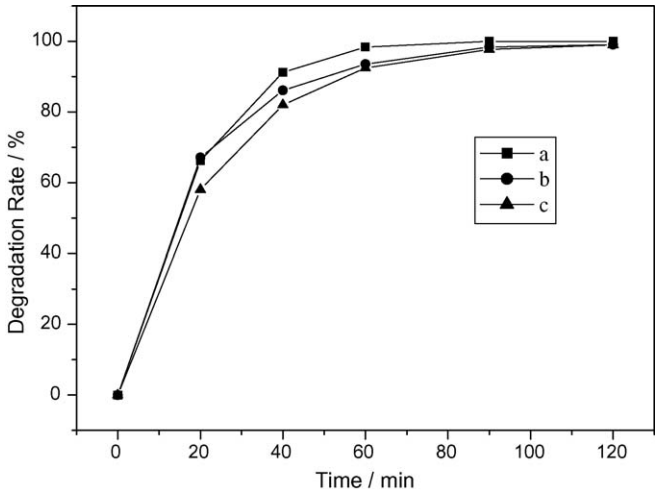

Fig. 6. Comparison of photocatalysis activity between (a) TiO_2–P25 and (b) 0.2 wt.% Cu-doped and (c) 0.5 wt.% Cu-doped.

distinctive peaks at 505, 330 and 215 nm, respectively, and the spectrum of acid red G in the visible region exhibits a main band with a maximum at 505 nm. The decrease of absorption peaks of acid red G at λ_{max} = 505 nm in the figure indicates a rapid degradation of azo dye. The peaks at 505 nm are also meaningful with respect to the nitrogen to nitrogen double bond (–N=N–) of the azo dye, as the most active site for oxidative attack.

3.3.2. *Effects of Cu-doping on photocatalytic activity of the catalysts*

The photodegradation rate of acid red G on Cu-doped catalysts under UV light irradiation within 120 min and the comparison of the photocatalytic activity of the catalysts are shown in Fig. 5. When using the pure $K_2Nb_4O_{11}$ catalyst, the absorbance of acid red G at 505 nm quickly decreased to 0.01 after 120 min under UV irradiation and the photodegradation rate of acid red G reached 96.83%, which means that the main part of the acid red G in the solution had been decomposed. When using the catalysts doped with 0.1, 0.2 and 0.5 wt.% copper, the photodegradation rates of acid red G had reached 91.99%, 93.35% and 92.46% after only irradiating 60 min and reached 97.76%, 99.03% and 99.03% after irradiating 120 min, and were higher than the pure $K_2Nb_4O_{11}$. However, as shown in the figure, the catalytic activity of $K_2Nb_4O_{11}$ catalyst would decrease with further increasing the concentration of Cu-doped. When using the catalysts doped with 1 wt.% copper, the photodegradation rate of acid red G were decreased to 54.25%. These results were contrasted with 6.21% degradation for the same experiments performed in the absence of photocatalysts, and the negligible 0.64% when the UV lamp had been switched off and the reaction in the present of photocatalysts was allowed to occur in the darkness. These experiments demonstrated that both UV light and photocatalysts are needed for the effective destruction of acid red G and the photocatalytic activity of Cu-doped $K_2Nb_4O_{11}$ is higher that of $K_2Nb_4O_{11}$.

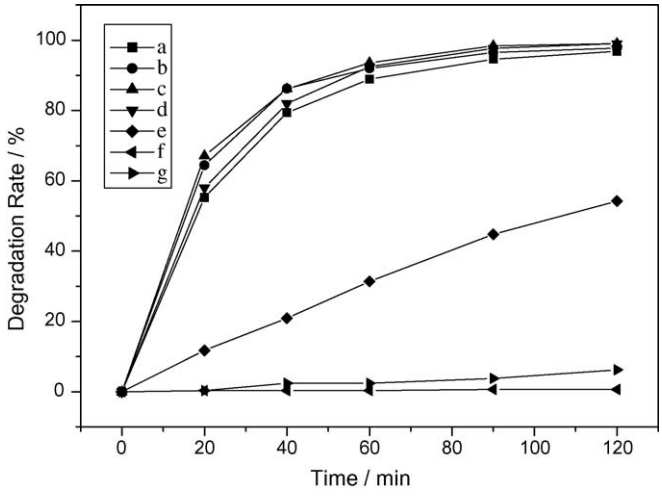

Fig. 5. Comparison of photocatalysis activity between $K_2Nb_4O_{11}$ and Cu-doped $K_2Nb_4O_{11}$: (a) $K_2Nb_4O_{11}$; (b) 0.1 wt.% Cu-doped; (c) 0.2 wt.% Cu-doped; (d) 0.5 wt.% Cu-doped; (e) 1 wt.% Cu-doped; (f) $K_2Nb_4O_{11}$ catalyst in the darkness; (g) the absence of photocatalysts.

As a comparison, the photodegradation of the 30mg/L acid red G over TiO_2–P25 and 0.2 wt.% Cu-doped $K_2Nb_4O_{11}$ and 0.5 wt.% Cu-doped $K_2Nb_4O_{11}$, respectively, are shown in Fig. 6. The catalyst dosage is 1 g/l. The surface areas of 0.2 wt.% Cu-doped $K_2Nb_4O_{11}$ and 0.5 wt.% Cu-doped $K_2Nb_4O_{11}$ and TiO_2–P25, which is 0.77 and 0.7 and 51 m^2/g, respectively. Although the surface areas of the 0.2 wt.% Cu-doped $K_2Nb_4O_{11}$ and the 0.5 wt.% Cu-doped $K_2Nb_4O_{11}$ are very lower, the photocatalytic activities of these compounds are close to that of TiO_2–P25. Moreover, TiO_2–P25 exhibited higher dispersion in the aqueous solution in comparison with the present Cu-doped $K_2Nb_4O_{11}$ photocatalysts, which was supposed to be one of the reasons for faster decomposition for acid red G. So, the photocatalytic activity of Cu-doped $K_2Nb_4O_{11}$ photocatalyst can be improved through increasing its surface area. The Cu-doped $K_2Nb_4O_{11}$ may find potentially application due to its chemical and structural stability in solution and easy preparation.

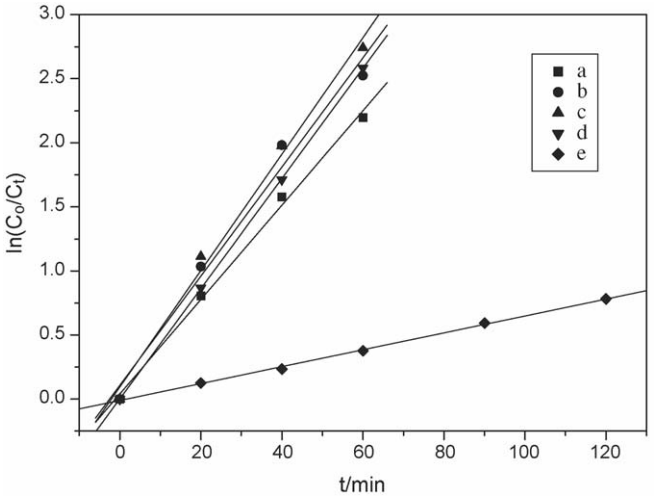

Fig. 7. Relationship between $\ln(C_0/C_t)$ and treatment time: (a) $K_2Nb_4O_{11}$; (b) 0.1 wt.% Cu-doped; (c) 0.2 wt.% Cu-doped; (d) 0.5 wt.% Cu-doped; (e) 1 wt.% Cu-doped.

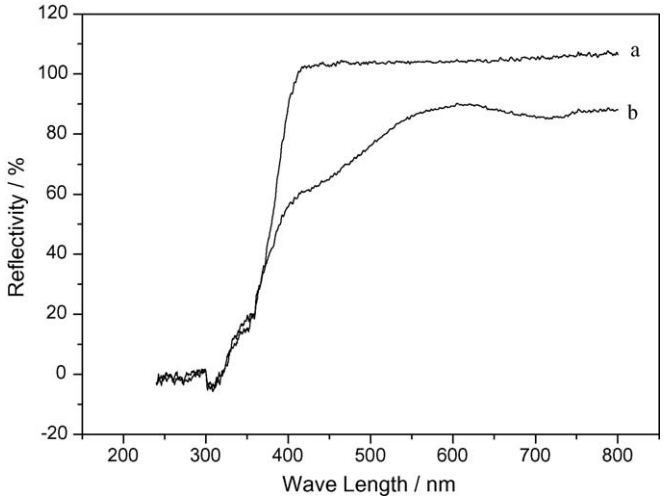

Fig. 8. Diffuse reflectance spectra of the photocatalysts: (a) $K_2Nb_4O_{11}$; (b) Cu-doped $K_2Nb_4O_{11}$.

3.3.3. Kinetics of photcatalytic degradation of acid red G

Most of the heterogenous photocatalytic degradation reaction follow Langmuir–Hinshelwood kinetic $\ln(C_0/C_t) = k(\text{min}^{-1})t + a$, [15] where k is the apparent reaction rate constant, C_0 the initial concentration, C_t the concentration at the reaction time of t and t is the reaction time. As Fig. 1 showed, the concentration (C) of acid red G has a good linear relation with the absorbance (A), thus, $\ln(C_0/C_t) \approx \ln(A_0/A_t)$, and the above can be approximated to $\ln(A_0/A_t) = k(\text{min}^{-1})t + a$, which belong to the first order kinetics, and this is confirmed by a nearly linear plot of $\ln(C_0/C_t)$ with t, as shown in Fig. 7. In the Fig. 5, we found that the acid red G could be almost completely degraded in 60 min by the catalysts except the catalysts doped with 1 wt.% Cu ions and therefore the last two points of the other four lines were omitted in Fig. 7.The kinetic parameters of each catalyst are listed in Table 1.

3.4. Diffuse reflectance spectra of the photocatalysts

The yield of photogenerated electron–hole pair first depends on the intensity of incident photons with energy exceeding or equalling to the photocatalyst band gap energy. Diffuse reflectance spectral analysis of the photocatalysts was determined by UV–vis spectrometer (UV-2100). Fig. 8 depicts diffuse reflectance spectra of photocatalysts of $K_2Nb_4O_{11}$ and 0.5 wt.% Cu-doped $K_2Nb_4O_{11}$. These spectra are noticeably different in the visible light region. The diffuse reflectance spectrum of Cu-doped $K_2Nb_4O_{11}$ has extended a red shift and increased absorbance in visible range. Yanagisawa et al. [16] found that the Cu-doped layered hydrogen titanates show the absorbance in the visible light region. The result reported by Chiang et al. [17] showed that the absorbance of copper-loaded TiO_2 exhibits a progressive increase. Here, the red shift and the increased absorbance in the visible region may be attributed to a charge transfer transition between the copper ion d electrons and the $K_2Nb_4O_{11}$ conduction or valence band.

3.5. ESR spectra of catalysts

Cu(II) is ESR active. Figs. 9 and 10 show ESR signal of doped Cu 0.5 wt.% catalyst at room temperature and at 77 K, respectively. The ESR result in Fig. 9 is similar to the results given by Chatterjee et al. [18–23], which shows the typical anisotropic ESR signal of Cu(II) ions and contain the characteristic copper hyperfine structure due to electron–nuclear interaction.. The paramagnetic sites of Cu(II) in the crystal structure of the catalyst is a distorted octahedral coordination [24–26].

3.6. XPS analysis of Nb

Fig. 11 shows the high-resolution XPS spectra of the Nb3d region the 0.2 wt.% Cu doped catalyst. The Nb3d region is composed of Nb3d5/2 peak and Nb3d3/2 peak. The Nb3d region

Table 1
Comparison of the kinetic parameters for the catalysts

Catalyst	The first order kinetic equation	Apparent reaction rate constant, k (min^{-1})	Correlation coefficient, R	Acid red G degradation, $t_{0.5}$ (min)
$K_2Nb_4O_{11}$	$\ln(C_0/C_t) = 0.0399 + 0.03683t$	0.03683	0.99829	17.73682
0.1 wt.% Cu-doped $K_2Nb_4O_{11}$	$\ln(C_0/C_t) = 0.10674 + 0.0426t$	0.0426	0.9911	13.76543
0.2 wt.% Cu-doped $K_2Nb_4O_{11}$	$\ln(C_0/C_t) = 0.09401 + 0.04543t$	0.04543	0.99626	13.18814
0.5 wt.% Cu-doped $K_2Nb_4O_{11}$	$\ln(C_0/C_t) = 0.00165 + 0.043t$	0.043	0.99998	16.08133
1 wt.% Cu-doped $K_2Nb_4O_{11}$	$\ln(C_0/C_t) = -0.0105 + 0.00659t$	0.00659	0.99924	106.7841

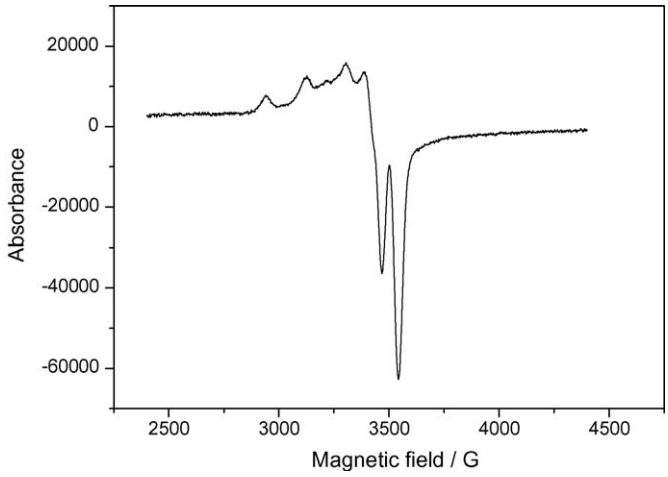

Fig. 9. The ESR spectra of 0.5 wt.% Cu-doped $K_2Nb_4O_{11}$ at room temperature.

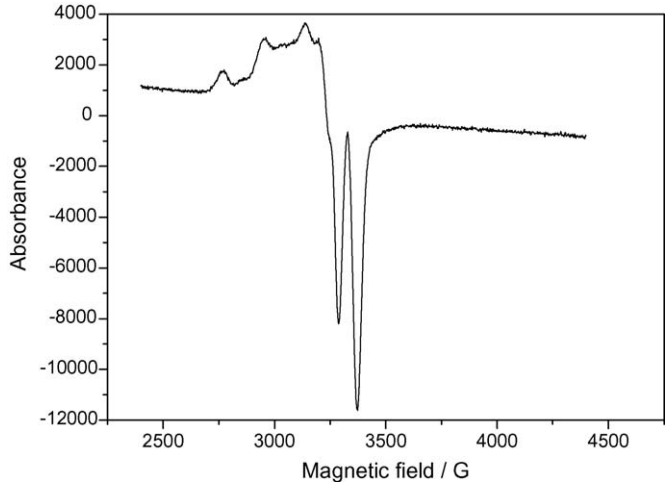

Fig. 10. The ESR spectra of 0.5 wt.% Cu-doped $K_2Nb_4O_{11}$ at 77 K.

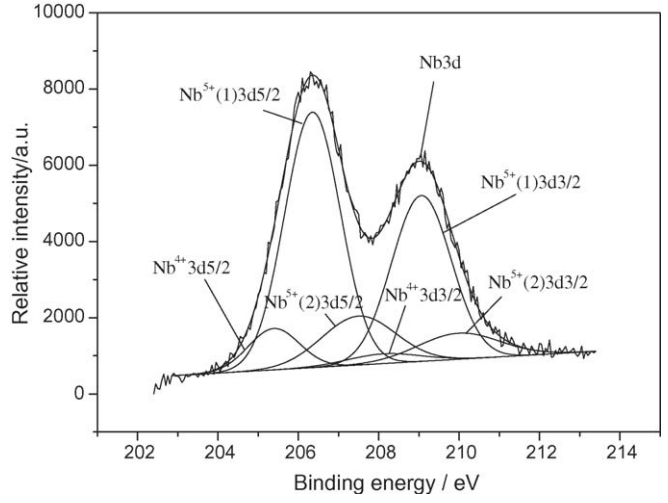

Fig. 11. High-resolution XPS spectra of the Nb3d region of the 0.2 wt.% Cu doped catalyst.

Table 2
Results of curve-fitting of the high resolution XPS spectra for theNb3d region

	$Nb^{5+}(1)$	$Nb^{5+}(2)$	$Nb^{4+}(3)$
Nb3d5/2 E_b (eV)	206.35	207.5	205.3
Nb3d3/2 E_b (eV)	209.06	209.99	208.12
r_i (%)	73.91	17.51	8.58

r_i (%) represents the ratio $A_i/\Sigma A_i$ (A_i is the area of each peak).

of the catalyst can be fitted by six peaks. Usually, the Nb3d5/2 binding energy of the Nb^{5+} in niobate is 206.5–207.2 eV, The Nb3d5/2 binding energy of the Nb^{4+} in niobate is about 205.5 eV [27–29]. The binding energy of the Nb^{4+} is lower than that of the Nb^{5+}. The two main peaks (206.35, 209.06) in Fig. 11 are attributed to the Nb3d5/2 peak and Nb3d3/2 peak of the $Nb^{5+}(1)$ in $Nb(1)O_6$ octahedra [30]. The higher binding energy peaks (207.5, 209.99) correspond to the Nb3d5/2 peak and Nb3d3/2 peak of the $Nb^{5+}(2)$ in $Nb(2)O_6$ octahedra. The lower binding energy peaks (205.3, 208.12) are the Nb3d5/2 peak and Nb3d3/2 peak of the $Nb^{4+}(3)$ at the site which is surrounded by three coplanar oxygen atoms at the apices of adjacent NbO_6 octahedra. Table 2 lists the results of curve fitting of XPS spectra for the catalyst, where r_i (%) shows the ratio of each kind contribution to the total of all the three kinds niobium contributions. The result of XPS analysis shows the niobium states on the surface of the catalyst. As can be seen in Table 2 and Fig. 11, the ratio of thee kinds of niobium in the catalyst is approximately consistent with the results reported by Kumuda and Kinamura and Ftini et al. [30,31]. By calculating, B, Kumuda and Kinamura and Ftini et al. think that the Nb^{4+} exists in the structure of $K_6Nb_{10.9}O_{30}$ and $K_{2.6}Nb_{11.6}O_{30}$, respectively [30,31]. The compound $K_6Nb_{10.9}O_{30}$ was synthesized in a stream hydrogen [30]. Here, we synthesized the compound $K_2Nb_4O_{11}$ in an air atmosphere. XPS analysis reveals Nb^{4+} exists in the structure of the compound $K_2Nb_4O_{11}$. The highly distorted surface NbO_6 octahedral sites always play an important role in heterogeneous catalysis [32]. The different binding energy of niobium in various niobium oxides determines its properties (among others the oxidation states and its stability). The stabilization of niobium influences the catalytic properties of Nb oxides. To achieve the material active in the redox catalysis, too high stability of Nb is unfavorable because it decreases the reducibility of niobium. The behavior of most oxidation catalysts can be interpreted within the framework of a redox mechanism (reduction–oxidation). The mobility of active oxygen is very important for the redox cycles as well. The mixed valence and Cu-doped of niobium increase the photocatalytic activity of the catalyst through enhancing the distortion of the NbO_6 octahedra and the mobility of active oxygen in the crystal structure of the catalyst [32].

3.7. Effects of Cu ions on the activity of catalysts

As shown in Fig. 5 and Table 1, the 0.2 wt.% Cu-doped $K_2Nb_4O_{11}$ shows a highest activity but the photodegradation rate of acid red G was found decreased with increasing the Cu dopant concentration. Effects of Cu ions in aqueous media

on the photodegradating of pollutants have been showed in some studies. The increased activity of catalyst was proposed to occur via the trapping of photogenerated electrons in the catalyst by Cu ions, thereby reducing the extent of deleterious electron–hole recombination [33]. Donia et al. [34] pointed out that the postulation to consider with regards to the role of Cu^{2+} in the enhancement of the photocatalytic degradation rates is the involvement of a ternary reactive complex readily form coordinated compounds. Such ternary complexes have been said to form between the copper ion, the organic or its oxidation intermediate, and an oxygen-containing species such as H_2O_2, O_2 of $O_2^{\bullet -}$. The ability of these compounds to take part in redox reactions, together with their photoreactivity have been said to be important for the photodegradation of organic pollutants in the environment. A catalytic effect of the Cu^{2+} ion was said to occur either through redox Cu^{2+}/Cu^{+} coupling reactions which inhibits the electron–hole recombination and the inner sphere mechanism of Cu^{2+} ions with the organic compounds, forming organo-metallic intermediates [35]. Lam et al. [36] studied effect of charge trapping species of cupric ions on the photocatalystic oxidation of resorcinol, the observed beneficial effect of cupric ions on the initial rate of resorcinol oxidation could be attributed to the formation of complex and its participation in the photo-redox cyclic reaction. The effect of copper ions on the formation of H_2O_2 over photocatalytic TiO_2 was investigated by Cai et al. [37] under an oxygen-purged solution, formation of H_2O_2 was increased dramatically up to 20 times by addition of a small amount of copper ions. The role of copper complex was studied by Cieśla et al. [38]. Copper participates in photo-redox cycle and its role cannot be ignored. The most importance part of the cycle is photo reduction of Cu(II) to Cu(I) induced by solar light and oxidation of ligands to the environmentally benign forms. The photocatalytic reaction in an aqueous TiO_2 suspension has been found enhanced by addition of copper metal powders loading on the TiO_2 particles [39]. The presence of Cu ions enhanced the photocatalytic removal efficiency of cyanide, the removed increased with increase on Cu:CN molar-ratio reaching a complete removal for both copper and cyanide at a ratio of 10:1 [40]. Copper(II) ions were found to accelerate the heterogeneous photocatalytic reduction of Cr(IV) in N_2-purged UV-irradiated TiO_2 suspensions [41].

Here, copper was doped in $K_2Nb_4O_{11}$ with TB structure. ESR result shows copper in Cu-doped $K_2Nb_4O_{11}$ mainly belongs to Cu^{II}. In the niobate with TB structure, one part of Cu^{II} may replace Nb^{5+} to form different valence isomorphism. On the other hand, the bond length of Cu–O can vary in a broad range, the other part of Cu^{II} ions occupy A_1 sites in the TB structure [42]. ESR result demonstrated that there are two kinds of Cu^{2+} ions with different chemical environment. In fact, Cu^{I} can exist in the TB structure as well, which may be to help exist Cu^{II}/Cu^{I} potential. UV–vis diffuse reflectance result showed doping copper changed the light absorbance properties of $K_2Nb_4O_{11}$ and onset of absorption extended a red shift. Zhang et al. [14] found that the absorption edges of the Cu-doped samples shifted to longer wavelength region and the best copper doping concentration is 1.45 at.%. The doped copper can provide a shallow trap for photo-generated electron and hole so as to inhibit the recombination and extend the lifetime of charge carrier. Therefore, the photodegradation rate could be enhanced consequently because more charge carriers are available. Araña et al. [43] thought formate molecules interact simultaneously with the dopants and surfacial Ti atoms yielding an intermediate species which play an important role in the phototacatalytic degradation mechanism or Cu oxides may act as receptors or transmitters of the TiO_2 photogenerated electrons. Chiang et al. [17] suggested that a Cu^{II} ion has an unfilled 3d shell ($t_{2g}^6 e_g^3$ configuration) and the reduction of Cu^{II} is thermodynamically feasible, it is valid to assume that electron can be trapped by $Cu^{II}O$ on the surface of catalyst. As a result of the electron trapping by $Cu^{II}O$, the rate of the electron–hole recombination reaction is slowed down and more holes are available for the redox reactions. Trapped electrons could also be consumed via the reduction of adsorbed oxygen molecules [44,45]. Since the solution in our experiments is continuously saturated with air by stirring, the majority of electrons trapped on the surface are dissipated through the oxygen reduction to form super oxide radical. Foster et al. [46] also reported that if oxygen is present in the system, the Cu^{I} could be oxidized back to Cu^{II}. As a result of the $Cu^{II}O \xrightarrow{e^-} Cu^{I}O \xrightarrow{O_2} Cu^{II}O$ sequential reactions, the electron hole recombination rate could be reduced.

However, these explanations seem to explain the enhancement at low Cu-doped concentration but do not account for the negative effect observed with further increasing the Cu-doped concentration. A plausible explanation for this phenomenon may be due to the short-circuiting mechanism of the coupled reaction, which occurs only at Cu^{II} concentration above a certain level. The coupled reaction is shown below as $Cu^{II} + 2e \rightarrow Cu^0$; $Cu^0 + 2h \rightarrow Cu^{II}$ [33]. At high loading of copper oxide, since the copper oxide was confined on the surface of catalysts, there is a high possibility for the trapped electrons to recombine with the holes. The oxidation of $Cu^{I}O$ to $Cu^{II}O$ by the photogenerated holes is expected to be faster than the photocatalytic redox reaction, since the former is simply a direct transfer of the trapped electron from $Cu^{I}O$ to the valence band hole. In that case the $Cu^{I}O$ might act as a recombination center and promote the recombination reaction [17]. Brezova et al. found that the inhibitory effect of Cu^{II} ions in phenol degradation was interpreted as the reduction of Cu^{II} ions from the solution and the subsequent deposition of CuO and Cu_2O on the surface of the catalysts [47].

4. Conclusion

It has been shown that the Cu-doped TB potassium niobate $K_2Nb_4O_{11}$ was synthesized by solid-state reaction method in air. The low concentration of Cu-doping can significantly increase the photocatalytic activity of $K_2Nb_4O_{11}$ catalyst. However, the photocatalytic activity of the catalyst was found decreased with increasing the concentration of copper dopant. The photodegradation reactions of acid red G by $K_2Nb_4O_{11}$ and Cu-doped $K_2Nb_4O_{11}$ follow the first order kinetics. The photocatalytic activities of the 0.2 wt.% Cu-doped $K_2Nb_4O_{11}$ and the 0.5 wt.% Cu-doped $K_2Nb_4O_{11}$ are close to that of TiO_2–P25.

XRD analysis and SEM analysis showed that the copper doping is good for the compounds to form tetragonal TB structure and improving the crystallinity of the compounds. The diffuse reflectance spectrum of Cu-doped $K_2Nb_4O_{11}$ has extended a red shift. XPS analysis confirmed that the niobium with mixed valence state, which may be advantage for increasing the photocatalytic activity of Cu-doped $K_2Nb_4O_{11}$, exists in the crystal structure of the Cu-doped compound $K_2Nb_4O_{11}$. The Cu-doped $K_2Nb_4O_{11}$ may find potential application in water treatment fields.

Acknowledgements

This work was financially supported by the National Natural Science Foundation of China (50472017). We thank Dr. Kumada N. and Dr. Nakato T. for the reprints of their articles.

References

[1] N. Daneshvar, H. Ashassi-Sorkhabi, A. Tizpar, Sep. Purif. Technol. 31 (2003) 153.
[2] Y.M. Slokar, A.M.L. Marechal, Dyes Pigm. 37 (1998) 335.
[3] C. Galindo, P. Jacques, A. Kalt, Chemosphere 45 (2001) 997.
[4] O. Tunay, I. Kabdasli, G. Eremektar, D. Orhon, Water Sci. Technol. 34 (1996) 9.
[5] D.F. Ollis, C. Hsiao, L. Budiman, C.L. Lee, J. Catal. 88 (1984) 89.
[6] J.M. Hermann, P. Pichat, J. Chem. Soc., Faraday Trans. I 76 (1980) 1138.
[7] Z.G. Zou, J.H. Ye, H. Arakawa, Int. J. Hydrogen Energy 28 (2003) 663.
[8] H. Kato, A. Kudo, J. Photochem. Photobiol. A: Chem. 145 (2001) 129.
[9] K. Domen, S. Ikeda, Microporous. Mater. 9 (1997) 253.
[10] M. Lundberg, M. Sundberg, J. Solid State Chem. 63 (1986) 216.
[11] J. Li, X.M. Chen, Y.J. Wu, J. Eur. Ceram. Soc. 22 (2002) 87.
[12] R.R. Neurgaonkar, W.K. Cory, J.R. Olier, Opt. Eng. 26 (1987) 392.
[13] W. Mu, J.M. Herrmann, P. Pichat, Catal. Lett. 3 (1989) 73.
[14] W.J. Zhang, Y. Li, S.L. Zhu, F.H. Wang, Catal. Today 93–95 (2004) 589.
[15] D.F. Ollis, Environ. Sci. Technol. 19 (1985) 480.
[16] M. Yanagisawa, S. Uchida, T. Sato, Int. J. Inorg. Mater. 2 (2000) 339.
[17] K. Chiang, R. Amal, T. Tran, Adv. Environ. Res. 6 (2002) 471.
[18] M. Chatterjee, T. Iwasaki, Y. Onodera, H. Hayashi, Y. Ikushima, T. Nagase, T. Ebina, Appl. Clay Sci. 25 (2004) 195.
[19] W. Böhlmann, A. Pöppl, D. Michel, Colloids Surf. A: Physicochem. Eng. Aspects 158 (1999) 235.
[20] T. Tanabe, T. Iijima, A. Koiwai, J. Mizuno, K. Yokota, A. Isogai, Appl. Catal. B: Environ. 6 (1995) 145.
[21] M.P. Attfield, S.J. Weigel, A.K. Cheetham, J. Catal. 172 (1997) 274.
[22] G. Centi, S. Perathoner, D. Biglino, E. Giamellot, J. Catal. 151 (1995) 75.
[23] V. Umamaheswari, A. Pöppl, M. Hartmann, J. Mol. Catal. A: Chem. 223 (2004) 123.
[24] C. Henriques, M.F. Ribeiro, C. Abreu, D.M. Murphy, F. Poignant, J. Saussey, J.C. Lavalley, Appl. Catal. B: Environ. 16 (1998) 79.
[25] J. Varga, J.B. Nagy, J. Halasz, I. Kiricsi, J. Mol. Struct. 410/411 (1997) 149.
[26] X.Q. Lu, W.D. Johnson, Sci. Total Environ. 203 (1997) 199.
[27] K. Tabata, T. Choso, Y. Nagasawa, Surf. Sci. 408 (1998) 137.
[28] K. Tabata, M. Kamada, T. Choso, H. Munakata, Appl. Surf. Sci. 125 (1998) 93.
[29] V.V. Atuchina, I.E. Kalabin, V.G. Kesler, N.V. Pervukhina, J. Electron Spectrosc. Relat. Phenom. 142 (2005) 129.
[30] N. Kumada, N. Kinamura, Eur. J. Solid State Inorg. Chem. 34 (1997) 65.
[31] M.M. Ftini, B. Ayed, A. Haddad, J. Chem. Cryst. 33 (2003) 123.
[32] M. Ziolek, Catal. Today 78 (2003) 47.
[33] H. Zhu, M.P. Zhang, Z.F. Xia, G.K.C. Low, Water Res. 29 (1995) 2681.
[34] D. Beydoun, H. Tse, R. Amal, J. Mol. Catal. A: Chem. 177 (2002) 265.
[35] E.C. Bulter, A.P. Davis, J. Photochem. Photobiol. A: Chem. 70 (1993) 273.
[36] S.W. Lam, K. Chiang, T.M. Lim, R. Amala, G.K.-C. Low, Appl. Catal. B: Environ. 55 (2005) 123.
[37] R.X. Cai, Y. Kubota, A. Fujishima, J. Catal. 219 (2003) 214.
[38] P. Cieśla, P. Kocot, P. Mytych, Z. Stasicka, J. Mol. Catal. A: Chem. 224 (2004) 17.
[39] K. Hirano, H. Asayama, A. Hoshino, H. Wakatsuki, J. Photochem. Photobiol. A: Chem. 110 (1997) 307.
[40] M.A. Barakat, Y.T. Chen, C.P. Huang, Appl. Catal. B: Environ. 53 (2004) 13.
[41] S. Goeringer, C.R. Chenthamarakshan, K. Rajeshwar, Electrochem. Commun. 3 (2001) 290.
[42] G.K. Zhang, L.Q. Qin, Mater. Chem. Phys. 74 (2002) 324.
[43] J. Araña, C. Garriga i Cabo, J.M. Doña-Rodríguez, O. González-Díaz, J.A. Herrera-Melián, J. Pérez-Peña, Appl. Surf. Sci. 239 (2004) 60.
[44] K. Okamoto, Y. Yamamoto, H. Tanaka, M. Tanaka, A. Itaya, Bull. Chem. Soc. Jpn. 58 (1985) 2015.
[45] H. Gerischer, A. Heller, J. Phys. Chem. 95 (1991) 5261.
[46] N.S. Foster, R. Noble, C.A. Koval, Environ. Sci. Technol. 27 (1993) 350.
[47] V. Brezova, A. Blazkova, E. Borosova, M. Ceppan, R. Fiala, J. Mol. Catal. A 98 (1995) 109.